

Unveiling the nature of electronic transitions in RbV_3Sb_5 with Avoided Level Crossing μSR

Pietro Bonfà,¹ Francis Pratt,² Diego Valenti,³ Ifeanyi John Onuorah,³ Anshu Kataria,³ Peter J. Baker,² Stephen Cottrell,² Andrea Capa Salinas,⁴ Stephen D. Wilson,⁴ Zurab Guguchia,⁵ and Samuele Sanna⁶

¹*Dipartimento di Fisica, Informatica e Matematica, Università di Modena e Reggio Emilia, Via Campi 213/a, 41125 Modena, Italy*

²*ISIS Pulsed Neutron and Muon Source, Rutherford Appleton Laboratory, Didcot OX11 0QX, U.K.*

³*Dipartimento di Scienze Matematiche, Fisiche e Informatiche, Università di Parma, I-43124 Parma, Italy*

⁴*Materials Department, University of California Santa Barbara, Santa Barbara, California 93106, USA*

⁵*PSI Center for Neutron and Muon Sciences CNM, 5232 Villigen PSI, Switzerland*

⁶*Dipartimento di Fisica e Astronomia "A. Righi", Università di Bologna, I-40127 Bologna, Italy*

(Dated: November 8, 2024)

Kagome superconductors AV_3Sb_5 provide a unique platform for studying the interplay between a variety of electronic orders, including superconductivity, charge density waves, nematic phases and more. Understanding the evolution of the electronic state from the charge density wave to the superconducting transition is essential for unraveling the interplay of charge, spin, and lattice degrees of freedom giving rise to the unusual magnetic properties of these nonmagnetic metals. Previous zero-field and high-field μSR studies revealed two anomalies in the muon spin relaxation rate, a first change at $T_{\text{CDW}} \sim 100$ K and a second steep increase at $T^* \sim 40$ K, further enhanced by an applied magnetic field, thus suggesting a contribution of magnetic origin. In this study, we use the avoided level crossing μSR technique to investigate charge order in near-zero applied field. By tracking the temperature dependence of quadrupolar level-crossing resonances, we examined the evolution of the electric field gradient at V nuclei in the kagome plane. Our results show a significant rearrangement of the charge density starting at T^* indicating a transition in the charge distribution, likely electronic in origin, well below T_{CDW} . These findings, combined with previous μSR , STM, and NMR studies, emphasize the intertwined nature of proximate phases in these systems, with the charge rearrangement dominating the additional increase in μSR relaxation rate below T^* .

INTRODUCTION

Transition-metal based kagome materials AV_3Sb_5 ($A = \text{K}, \text{Rb}, \text{Cs}$) have generated increasing interest in the scientific community owing to the diverse physical properties that have been observed, including nontrivial band topology, anomalous Hall effect (AHE) [1], and an intriguing interplay between superconductivity (SC) and unconventional charge density wave (CDW) [2].

Despite numerous theoretical and experimental investigations, even when focusing only on the normal state, the current understanding of the cascade of transitions characterizing the electronic behavior of these compounds remains incomplete. Initially, with decreasing temperature, a CDW transition occurs at $T_{\text{CDW}} \sim 78 - 102$ K depending on the alkali metal [3]. In this phase, the hexagonal lattice with $P6/mmm$ symmetry undergoes a distortion involving the formation of V hexamers and trimers which produces the so called Tri-Hexagonal structure (TrH) in the kagome planes with the crystal adopting the $Fmmm$, $Cmmm$ or $C2/m$ space group symmetry [4–9]. This phase also features an additional modulation along the c axis, likely due to a staggered displacement pattern of the kagome layers, although some uncertainty on the mutual arrangement of these planes persists [4, 10–13], probably owing to the delicate competition between CDW orders with different stacking modulations [14].

At lower temperature, the presence of a nematic transition breaking the C_6 symmetry of the kagome planes [15] has been reported for CsV_3Sb_5 [16], but its nature (and existence) is still debated [2, 17–21]. Notably, this and other symmetry-breaking charge orders were identified only in CsV_3Sb_5 [22],

while no other charge order transitions between T_{CDW} and T_{SC} have been reported for $A = \text{K}, \text{Rb}$.

A distinctive feature of kagome systems is the potential for time-reversal symmetry (TRS) breaking in the normal state, as initially suggested by high-field scanning tunneling microscopy [23], along with evidence from a combination of zero-field and high-field muon spin relaxation (μSR) [24], supported by various experiments [25–28] such as magneto-chiral anisotropy, the anomalous Hall effect [1], and magneto-optical Kerr effect (MOKE) measurements [29].

Several theoretical studies [30–38] attribute the TRS-breaking signal to orbital current phases. Furthermore, polarized neutron diffraction experiments hint at the presence of a weak magnetic signal in the second Brillouin zone at $M_2 = (1/2, 1/2, 0)$ [39]. This finding, interpreted as loop current patterns localized on vanadium triangles, reports an ordered orbital magnetic moment of at most $0.02 \mu_B$ per vanadium triangle.

However, whether the system breaks TRS spontaneously, i.e. in zero applied magnetic field, has been challenged by MOKE [40–42] studies that have reported no observable Kerr response in zero field (ZF). A recent analysis of transport properties suggests that the origin of the controversial reports is an extraordinary sensitivity to weak perturbations, in particular strain and magnetic fields [43]. This is in line with earlier high-field μSR experiments revealing a significant enhancement of muon relaxation rates with out-of-plane magnetic fields, and with high-field STM experiments, which showed charge density wave (CDW) intensity switching under out-of-plane magnetic fields and in-plane electric fields, implying an unusual piezo-magnetic response [27].

ZF- μ SR is one of the cleanest methods to identify TRSB owing to the possibility of performing ZF experiments on bulk samples and thanks to its sensitivity to extremely small magnetic fields [44]. For this reason, a large number of experiments have been conducted [45, 46]. The central quantity investigated during the experiment is the polarization function of the muon, defined as the time evolution of the muon spin projected along the direction of the positron detectors, which is obtained by exploiting the asymmetry in the weak decay of the muon. This time evolution encodes the details of the interaction between the muon spin, the neighboring nuclear spins and electronic (spin or orbital) moments, making it a local probe for both electronic and structural transitions.

Previous ZF μ SR studies [22, 24, 46, 47] on RbV_3Sb_5 have revealed a two-step increase in the relaxation rate, a smaller one at $T_{CDW} \approx 100$ K and a second one at $T^* \lesssim 50$ K. The increase in the relaxation rate corresponds to internal fields on the order of 0.01 mT. The effect is enhanced under an applied magnetic field, thus suggesting a magnetic contribution to the relaxation. A significant enhancement of the relaxation is also detected near the surface region of RVS, specifically within 30 nm from the surface. A similar two-step increase in the relaxation rate was observed in the sister compound CsV_3Sb_5 , at $T_{CDW} \approx 90$ K and at $T^* \approx 30$ K. However, the nature of the additional increase in the relaxation rate below T^* remains uncertain, leaving open the question of whether this increase is magnetic in origin or if changes in the charge order also contributes.

Muons serve as exceptional probes not only for magnetism but also for investigating charge order. In particular, the experimental technique known as Avoided Level Crossing (ALC) μ SR enables the study of charge distribution evolution by monitoring changes in the Electric Field Gradient (EFG) tensor at nuclei with spin $I > 1/2$, located near the muon. This information is obtained indirectly through the dipolar coupling between the muon and quadrupole-active nuclei. The idea behind ALC was first proposed by Abragam [48], who noted that nuclear quadrupole splittings could be measured indirectly with μ SR, by finely tuning the muon Zeeman energy to match a nuclear quadrupolar splitting, thus resulting in a cross relaxation between the spins known as muon quadrupole level crossing resonance (μ -QLCR or simply QLCR). As a consequence, one can selectively probe different nuclei by matching different quadrupolar energies, whereas in ZF experiments the nuclear contribution to the polarization function is dominated by the dipolar interaction between the muon and the nearest nuclei. This is indeed the strategy adopted in this work and a nice review of this approach is presented in Ref. [49].

RESULTS

For all experiments we used finely ground RbV_3Sb_5 powders, identical to the sample in Ref. [50]. Both the ZF and the ALC acquisitions have been carried out using the EMU spectrometer [51] at the ISIS pulsed muon facility.

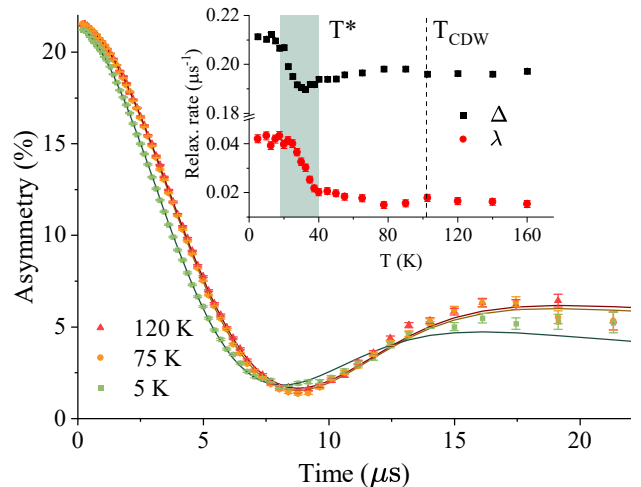


FIG. 1. The ZF- μ SR spectra of RbV_3Sb_5 . In the main panel, three high-statistics acquisitions showing the evolution of the asymmetry as a function of the temperature. A tiny difference is observed between signals above (120 K) and below (75 K) the CDW transition (102 K). A noticeably faster relaxation is instead observed in the measurement performed at 5 K. The continuous lines are best-fits to Eq. 1. The inset shows the temperature evolution of the fitting parameters resulting from the analysis described in the main text.

Zero Field μ SR

The ZF- μ SR data are shown in Fig. 1. The asymmetry has been analyzed with best fits to the equation

$$A(t) = A_0 \left[\frac{1}{3} + \frac{2}{3} (1 - \Delta^2 t^2) e^{-\Delta^2 t^2 / 2} \right] e^{-\lambda t} + B \quad (1)$$

for consistency to the previous literature [46, 47, 52]. In Eq. 1, A_0 is the relaxing asymmetry, B is a baseline, and the function in square brackets is the Kubo-Toyabe (KT) function [44] characterized by a relaxation rate Δ and multiplied by an additional Lorentzian relaxation, parameterized by λ . This phenomenological approach matches very well with the experimental data at short time, while small deviations are observed for $t > 13 \mu\text{s}$ in the $T = 75$ and 120 K measurements. A dramatic discrepancy is instead observed at 5 K for $t > 10 \mu\text{s}$, showing the limits of the phenomenological description based on Eq. 1. Notably, the tail of the 5 K signal remains relatively flat, indicating a lack of dynamic effects.

It should be noted that the KT function in Eq. 1 arises from a semi-classical description of the muon-nuclei interaction. For this reason, an additional relaxation contribution and a (temperature-dependent) baseline B are required. Departures from the semi-classical prediction are common and are generally found in the long-time tail, as shown for example in Ref. [53], though relevant effects can also take place at shorter times [54, 55]. A very accurate prediction of the ZF muon polarization function above T^* can be obtained from first principles modeling of the muon site and its interaction with the neighboring nuclei, when the entire description is performed

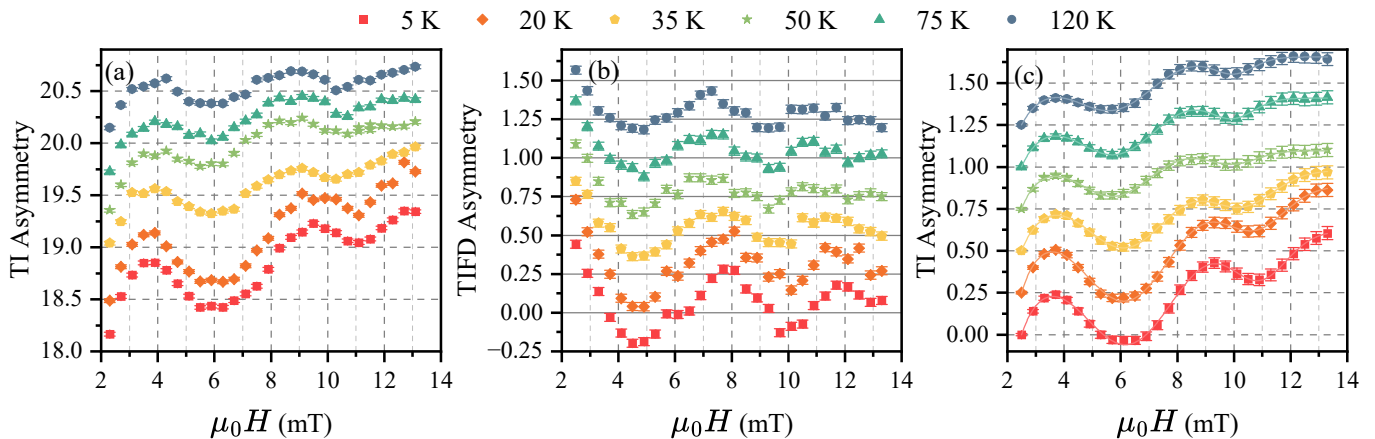


FIG. 2. ALC results and analysis. In panel (a), the time-integrated asymmetry as a function of the temperature. Results are reported with vertical offsets for clarity. In (b), the time-integrated-field-differential acquisitions. The same vertical offset is used. In (c) the numerical integration of the results shown in panel (b). The continuous lines are best fit to the data according to Eq. 2 described in the main text.

at the quantum mechanical level. These results have already been presented in Ref. [50], together with a detailed description of the muon sites, which reveals that the ZF signal is most sensitive to the in-plane Sb atoms through a simple dipolar interaction between the muon spin and the nearest neighbouring isotopes ($m_{121\text{Sb}} = 3.36\mu_P$, $m_{123\text{Sb}} = 2.55\mu_P$ and $d_{\mu-\text{Sb}} \sim 1.7 \text{ \AA}$) Sb isotopes, while the coupling with the V nuclei forming the kagome lattice is much weaker ($m_{\text{Sb-V}} = 5.15\mu_P$ and $d_{\mu-\text{V}} \sim 3.5 \text{ \AA}$). However, in the following discussion, we still opt for the phenomenological model due to its simplicity and effectiveness in capturing the transitions observed in the ZF data.

The inset of Fig. 1 reports the temperature evolution of λ and Δ obtained from best-fits of the measurements performed in the temperature interval 5 – 160 K. Two transitions can be detected, at about $T_{\text{CDW}} = 100 \text{ K}$ and $T^* = 40 \text{ K}$. The trend follows what has been already reported in literature [47]. As can be appreciated from the main panel Fig. 1, the transition at T_{CDW} has a small effect on the polarization function of the muon. On the other hand, a marked change takes place below T^* as shown also by the difference between the raw data acquired at 5 and 75 K (Fig. 1 main panel).

The extended time window of our new measurements provides a more detailed picture of the evolution of the μSR signal as a function of the temperature. From the phenomenological analysis, considering both λ and Δ , the broad transition that starts at $T^* = 40 \text{ K}$ is finally completed at $T \sim 20 \text{ K}$, where both the relaxation coefficients become temperature independent.

Avoided Level Crossing

Longitudinal field ALC experiments have been performed with $\mu_0 H$ ranging from 2.3 to 13.1 mT. The asymmetry within the time interval 1.44 μs to 30 μs is integrated in time (TI) and

shown in Fig. 2a. For $\mathbf{B} \rightarrow 0$ the signal decays owing to the dipolar interaction between the muon and the neighbouring nuclei and the TI asymmetry reduces accordingly. With increasing longitudinal fields, two resonances at about 6 and 11 mT are clearly observed, especially at low temperature.

In order to reduce the noise of the data, we employ a field-differential approach [56], where the external magnetic field is varied by $\pm 0.2 \text{ mT}$ during the acquisition, thus removing the instabilities of the beam affecting the raw data. The difference of the asymmetries acquired in the two conditions represents the finite difference approximation of the derivative of the signal as a function of the applied magnetic field [56]. The time-integrated field-differential (TIFD) signal is reported in Fig. 2b. These curves already show a clear temperature dependence, but the main result of this procedure are the resonances shown in Fig. 2c obtained by numerical integration.

The numerically integrated TIFD data, $I(B)$, are fitted to the equation

$$I(B) = I_0 \left(1 - \frac{\tau}{B^N} \right) - \sum_{i=1}^2 \frac{A_i}{\sigma_i \sqrt{2\pi}} \exp \left(-\frac{1}{2} \frac{(B - B_i^{\text{res}})^2}{\sigma_i^2} \right) \quad (2)$$

where in the first two terms, τ and N , are used to approximate the exact description [57] of the time integrated polarization function of pure dipolar origin in longitudinal applied field. The observed level-crossing resonances are instead captured with two Gaussian functions, each characterized by three parameters: A , B^{res} and σ respectively the area, the average resonance field and the width of the resonance.

The results of the fit are shown in Fig. 3. Surprisingly, the CDW transition has a very slight effect, if any, on the resonance parameters, while sizable deviations are observed for $T \lesssim T^*$. Indeed the area of both resonances, shown in Fig. 3a, increases below 40 K and it remains constant between 20 and 5 K. The average resonant fields, shown in Fig. 3b, also display a clear shift of the order of 1 mT when the temperature

drops below 40 K. Finally, a similar temperature dependence is also observed for the width of the resonance peaks in panel (c), although the actual trend for the second resonance is impaired by the large uncertainty of this parameter.

DISCUSSION

In order to obtain a microscopic description of the ALC results we started from the Plane Wave (PW) based DFT simulations published in Refs. [50, 58]. As already discussed in [50], in the staggered TrH structure there are 3 symmetry inequivalent muon sites, but the neighborhoods of the muon are always very similar, i.e. the distance between the muon and the various atoms of the system change very little between the sites. These simulations also provide information on the perturbation introduced by the muon on the EFG at the neighboring sites. As expected, we find that the EFG of the nearest neighbor (NN) of the muon, the in-plane Sb atom, is strongly perturbed by the presence of the positive interstitial charge. In contrast, the EFG at the second NN, the Rb atom, is much less affected, with variations of V_{zz} smaller than 10% and even less for the V atoms that are more than 3.5 Å away from the muon (see Supplemental Material for details). This preliminary analysis provides valuable information towards the identification of the nuclei involved in a QLCR producing the experimental signal. It is found indeed that, for the field range of the measurement, a hexagon of six V atoms close to the muon site contribute most significantly to the QLCR spectra (see SM).

While PW based results represent a good starting point, their accuracy is lower than full-potential APW based simulations in the description of charge distributions at nuclear sites. In light of this, to obtain more accurate predictions, we adopt the Full-Potential APW-based estimate for the EFGs at V atoms in the TrH phase already published in Refs. [7, 59] while maintaining the equilibrium distances between the muon and the atoms obtained with the PW-based supercell simulation [50, 58]. By doing so we neglect the staggering along the c axis and the perturbation introduced by the muon on the EFG (which is very limited for V atoms, see SM). In the TrH structure there are only two symmetrically distinct sites and we compute, for each of them, the polarization function arising from the interaction between the muon and six NN V atoms, using the method introduced by Celio [60, 61]. To check for convergence of our simulations, we also include the NN Sb atom (the ^{121}Sb isotope is only considered). The nuclear quadrupolar coupling constant C_Q , defined as

$$C_Q = e_0 V_{zz} Q / h \quad (3)$$

where $Q = -0.043$ barn is the quadrupolar moment of ^{51}V and V_{zz} is the largest eigenvalue of the EFG tensor, is predicted to be $C_Q^{APW} = 6.85$ MHz, and the asymmetry parameter $\eta = (V_{xx} - V_{yy})/V_{zz}$ is $\eta^{APW} = 0.43$. The inclusion of the NN Sb in the Hilbert space negligibly affects the resonances and only alters the TI Asymmetry for $B \rightarrow 0$ (not shown) [62].

The resulting curves, shown in Fig. 4a, match very well with the experimental results above T^* . In addition, they reveal why this probe is insensitive to the CDW order: the EFG at V nuclei varies very little across the transition and the geometrically equivalent V atoms in the high temperature phase split into two inequivalent sites with equal multiplicity. For the first(second) set, V_{zz} is slightly decreasing(increasing) with respect to the value in the hexagonal phase. The resulting signal displays QLCR that are just very slightly broader than the ones of the hexagonal phase, with the only noticeable difference visible at about 11 mT.

Unfortunately, this approach is computationally demanding and prevents fitting the microscopic QLCR parameters C_Q and η to the experimental data. Therefore, since the muon is close to the centre of the hexagon and the magnitudes of the EFG parameters are similar for all six, for fitting purposes we took one V site as representative and calculated the polycrystalline averaged QLCR spectrum versus η with the principal axis of the field gradient aligned at 90° to the muon vector. The QLCR for the six V sites was then evaluated by scaling the resonance amplitude by a factor of six. Finally, a cubic background is added to account for the minor contributions from other nuclei. This approach yields an average trend and assumes that the dipolar interactions between V nuclei are not significant compared to the dipolar interaction between the muon and each individual V. This model requires a reduced Hilbert space (consisting of the muon and one V atom at a time), allowing us to extract an averaged trend for the parameters describing the dipolar and quadrupolar coupling of the V nuclei with the muon and the surrounding electronic charge, respectively.

In order to obtain a quantitative comparison with the experiment, we fit the time integrated asymmetry (instead of the numerical integration of Fig 2c) and we report the results with respect to the *ab initio* prediction. The comparison is made through the NQCC factor, defined as $f_{NQCC} = C_Q^{\text{Exp}}/C_Q^{\text{PW}}$ and the scaling factor A required to match the amplitude of the experimental resonance with the predicted one. The asymmetry parameter, η , is instead reported directly for simplicity of presentation [63].

The results of the fit are shown in Fig. 4b. At high temperature, the resonance frequency is very well estimated ($f_{NQCC} \sim 0.97$) while the amplitude of the resonance is slightly underestimated ($A \sim 0.75$). The asymmetry parameter η is close to the experimental result [12] and to APW based estimates. Both A and f_{NQCC} increase as temperature decreases, and the trend of the microscopic parameters roughly aligns with the phenomenological analysis in Fig.3. Interestingly, the variation of V_{zz} at V nuclei probed by muons, of the order of 5%, is slightly larger than the one reported by high field NMR measurements in CsV_3Sb_5 (see SI of Ref. [17]).

With the microscopic origin of the QLCR clarified, we now turn our attention to the relationship between these findings and previous zero-field (ZF) measurements.

Remarkably, the ZF muon-spin relaxation rates Δ and σ (inset of Fig. 1), the phenomenological ALC parameters A_i ,

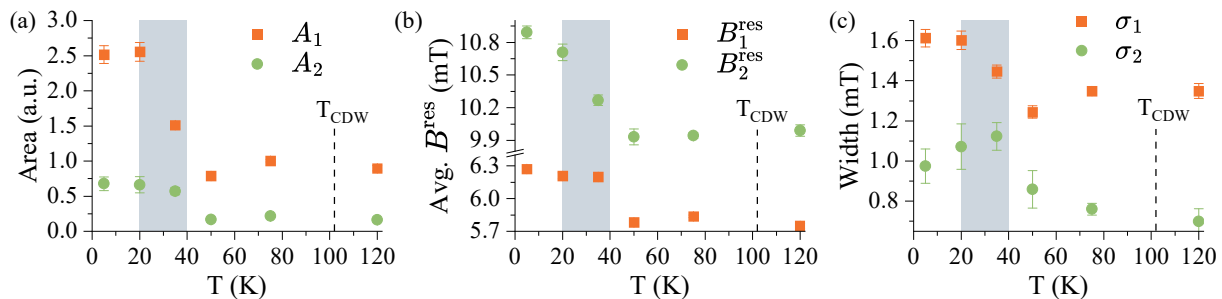


FIG. 3. Parameters obtained from best-fit curves shown in Fig. 2c. In panel (a) the area of the Gaussian used to describe the two resonances. In (b) the resonant field, in (c) the width of the two Gaussian functions. The gray shadow shows the same temperature interval displayed in Fig. 1 where the second low-temperature transition takes place according to ZF results.

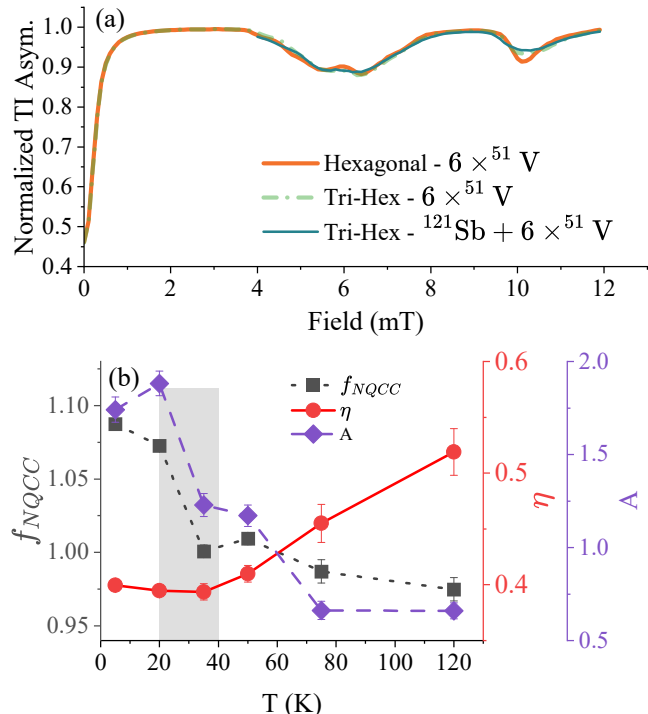


FIG. 4. Panel (a): predicted resonances for $T > T_{CDW}$ in the Hexagonal structure and for the low temperature TrH structure (neglecting the modulation along the c axis). The legend also reports the cluster of nuclei included in the simulation. The EFGs at V and Sb sites are obtained from a full-potential DFT-based prediction. Panel (b): results of the fit of TI asymmetry to the microscopic model described in the main text.

B_i , and σ_i (Fig. 3), and the results of the microscopic model (Fig. 4b) exhibit similar temperature dependence, as highlighted by the shaded region. A key question is whether the ALC resonance field shift, shown in Fig. 3b, can be attributed to an additional field generated by weak magnetic interactions. The ZF relaxation rate increasing by $\delta\lambda \lesssim 0.03 \mu\text{s}^{-1}$, corresponds to a local field increase of $\delta B = \delta\lambda/(\gamma_\mu) \sim 0.035 \text{ mT}$ [64]. However, the observed shift in ALC resonance is more than an order of magnitude larger. Therefore, the contribu-

tion to the increase of ALC resonance field from magnetic coupling between the muon and the electronic channel via orbital or spin magnetism is minimal. We conclude that the increase of the resonant field is primarily due to a shift in nuclear quadrupolar energy levels, caused by charge redistribution at the V sites, indicating the presence of a transition in the charge channel setting in before the onset of superconductivity.

The key question now is what drives this charge redistribution. Given the lack of thermodynamic evidence for a transition at $T^* \sim 40 \text{ K}$ and the absence of major structural distortions, this cannot be attributed to simple structural changes. Notably, NMR experiments and STM measurements in CsV_3Sb_5 and KV_3Sb_5 [17, 19, 65] have reported rotational symmetry broken states stabilized well below the CDW order. It is plausible to assume that the charge redistribution observed below $T^* \sim 40 \text{ K}$ in RbV_3Sb_5 shares a similar origin with CsV_3Sb_5 and KV_3Sb_5 hinting at electronic nematicity.

CONCLUSIONS

We have presented ZF and ALC μSR experiments performed on RbV_3Sb_5 . With the latter technique we investigated the evolution of charge order in the kagome plane. Our results reveal a significant rearrangement of charge density around the muon below $T^* \sim 40 \text{ K}$, an effect that matches with the upturn of the muon relaxation rate observed in ZF- μSR . This uncovers a hitherto unnoticed charge order transition well below the onset of the CDW and before the system enters the superconducting state and suggests that a non-trivial evolution of the local charge/electronic landscape is the primary origin for the phenomenology observed in zero and near-zero field conditions. These findings, combined with previous high-field μSR , NMR, STM and transport studies, demonstrate that the charge and spin channels are strongly intertwined in these materials.

Furthermore, this study highlights the effectiveness of ALC μSR measurements as a powerful tool for probing electronic orders. Additional experimental and computational investigations, potentially utilizing resonances of other quadrupolar nuclei (Rb, Sn, Cs, K), will be essential to further elucidate

the microscopic long-range order below T^* in this and related compounds.

ACKNOWLEDGMENTS

We thank Roberto De Renzi and Giuseppe Allodi for insightful discussions. The computational resources were provided by the SCARF cluster of the STFC Scientific Computing Department and by the IS CRA initiative of CINECA with project IsCb6_TRSBKS. Work in Parma was funded by the PNRR MUR project ECS-00000033-ECOSISTER. IO acknowledges support by University of Parma through the action Bando di Ateneo 2023 per la ricerca. SDW and ACS gratefully acknowledge support via the UC Santa Barbara NSF Quantum Foundry funded via the Q-AMASE-i program under award DMR-1906325.

-
- [1] S.-Y. Yang, Y. Wang, B. R. Ortiz, D. Liu, J. Gayles, E. Derunova, R. Gonzalez-Hernandez, L. Šmejkal, Y. Chen, S. S. P. Parkin, S. D. Wilson, E. S. Toberer, T. McQueen, and M. N. Ali, *Science Advances* **6**, 10.1126/sciadv.abb6003 (2020).
- [2] M. Frachet, L. Wang, W. Xia, Y. Guo, M. He, N. Maraytta, R. Heid, A.-A. Haghighirad, M. Merz, C. Meingast, and F. Hardy, *Phys. Rev. Lett.* **132**, 186001 (2024).
- [3] M. Wenzel, B. R. Ortiz, S. D. Wilson, M. Dressel, A. A. Tsirlin, and E. Uykur, *Phys. Rev. B* **105**, 245123 (2022).
- [4] H. Li, T. T. Zhang, T. Yilmaz, Y. Y. Pai, C. E. Marvinney, A. Said, Q. W. Yin, C. S. Gong, Z. J. Tu, E. Vescovo, C. S. Nelson, R. G. Moore, S. Murakami, H. C. Lei, H. N. Lee, B. J. Lawrie, and H. Miao, *Phys. Rev. X* **11**, 031050 (2021).
- [5] A. Subedi, *Phys. Rev. Mater.* **6**, 015001 (2022).
- [6] H. Tan, Y. Liu, Z. Wang, and B. Yan, *Phys. Rev. Lett.* **127**, 046401 (2021).
- [7] J. Frassinetti, P. Bonfà, G. Allodi, E. Garcia, R. Cong, B. R. Ortiz, S. D. Wilson, R. De Renzi, V. F. Mitrović, and S. Sanna, *Phys. Rev. Res.* **5**, L012017 (2023).
- [8] L. Kautzsch, B. R. Ortiz, K. Mallayya, J. Plumb, G. Pokharel, J. P. C. Ruff, Z. Islam, E.-A. Kim, R. Seshadri, and S. D. Wilson, *Phys. Rev. Mater.* **7**, 024806 (2023).
- [9] A. Ptok, A. Kobiałka, M. Sternik, J. Łażewski, P. T. Jochym, A. M. Oleś, and P. Piekarczyk, *Phys. Rev. B* **105**, 235134 (2022).
- [10] B. R. Ortiz, S. M. L. Teicher, L. Kautzsch, P. M. Sarte, N. Ratcliff, J. Harter, J. P. C. Ruff, R. Seshadri, and S. D. Wilson, *Phys. Rev. X* **11**, 041030 (2021).
- [11] Q. Stahl, D. Chen, T. Ritschel, C. Shekhar, E. Sadrollahi, M. C. Rahn, O. Ivashko, M. v. Zimmermann, C. Felser, and J. Geck, *Phys. Rev. B* **105**, 195136 (2022).
- [12] X. Zhang, Y. Li, J. Zheng, F. Zhou, Q. Wu, X. Xi, Y. Lau, Z. Wang, and W. Wang, *Applied Physics Letters* **124**, 093106 (2024).
- [13] V. Scagnoli, L. J. Riddiford, S. W. Huang, Y.-G. Shi, Z. Tu, H. Lei, A. Bombardi, G. Nisbet, and Z. Guguchia, *Journal of Physics: Condensed Matter* **36**, 185604 (2024).
- [14] C. Park and Y.-W. Son, *Nature Communications* **14**, 10.1038/s41467-023-43170-w (2023).
- [15] It should be noted that, while at T_{CDW} the rotational symmetry of the system changes from $C6$ to $C2$ owing to the staggered order along c , the kagome layers retain the original sixfold rotational symmetry. Yet, at lower temperature, the $C6$ symmetry of the 2D kagome layer may also be broken by the so called “strong” nematic state (to distinguish it from the “weak” nematic state realized at T_{CDW} [66]).
- [16] H. Zhao, H. Li, B. R. Ortiz, S. M. L. Teicher, T. Park, M. Ye, Z. Wang, L. Balents, S. D. Wilson, and I. Zeljkovic, *Nature* **599**, 216–221 (2021).
- [17] L. Nie, K. Sun, W. Ma, D. Song, L. Zheng, Z. Liang, P. Wu, F. Yu, J. Li, M. Shan, D. Zhao, S. Li, B. Kang, Z. Wu, Y. Zhou, K. Liu, Z. Xiang, J. Ying, Z. Wang, T. Wu, and X. Chen, *Nature* **604**, 59–64 (2022).
- [18] Y. Sur, K.-T. Kim, S. Kim, and K. H. Kim, *Nature Communications* **14**, 10.1038/s41467-023-39495-1 (2023).
- [19] H. Li, H. Zhao, B. R. Ortiz, Y. Oey, Z. Wang, S. D. Wilson, and I. Zeljkovic, *Nature Physics* **19**, 637 (2023).
- [20] Z. Liu, Y. Shi, Q. Jiang, E. W. Rosenberg, J. M. DeStefano, J. Liu, C. Hu, Y. Zhao, Z. Wang, Y. Yao, D. Graf, P. Dai, J. Yang, X. Xu, and J.-H. Chu, *Phys. Rev. X* **14**, 031015 (2024).
- [21] T. Asaba, A. Onishi, Y. Kageyama, T. Kiyosue, K. Ohtsuka, S. Suetsugu, Y. Kohsaka, T. Gaggli, Y. Kasahara, H. Murayama, K. Hashimoto, R. Tazai, H. Kontani, B. R. Ortiz, S. D. Wilson, Q. Li, H. H. Wen, T. Shibauchi, and Y. Matsuda, *Nature Physics* **20**, 40–46 (2024).
- [22] S. D. Wilson and B. R. Ortiz, *Nature Reviews Materials* **9**, 420–432 (2024).
- [23] Y.-X. Jiang, J.-X. Yin, M. M. Denner, N. Shumiya, B. R. Ortiz, G. Xu, Z. Guguchia, J. He, M. S. Hossain, X. Liu, J. Ruff, L. Kautzsch, S. S. Zhang, G. Chang, I. Belopolski, Q. Zhang, T. A. Cochran, D. Multer, M. Litskevich, Z.-J. Cheng, X. P. Yang, Z. Wang, R. Thomale, T. Neupert, S. D. Wilson, and M. Z. Hasan, *Nature Materials* **20**, 1353–1357 (2021).
- [24] C. Mielke, D. Das, J.-X. Yin, H. Liu, R. Gupta, Y.-X. Jiang, M. Medarde, X. Wu, H. C. Lei, J. Chang, P. Dai, Q. Si, H. Miao, R. Thomale, T. Neupert, Y. Shi, R. Khasanov, M. Z. Hasan, H. Luetkens, and Z. Guguchia, *Nature* **602**, 245–250 (2022).
- [25] D. Chen, B. He, M. Yao, Y. Pan, H. Lin, W. Schnelle, Y. Sun, J. Gooth, L. Taillefer, and C. Felser, *Phys. Rev. B* **105**, L201109 (2022).
- [26] C. Guo, C. Putzke, S. Konyzheva, X. Huang, M. Gutierrez-Amigo, I. Errea, D. Chen, M. G. Vergniory, C. Felser, M. H. Fischer, T. Neupert, and P. J. W. Moll, *Nature* **611**, 461–466 (2022).
- [27] Y. Xing, S. Bae, E. Ritz, F. Yang, T. Birol, A. N. Capa Salinas, B. R. Ortiz, S. D. Wilson, Z. Wang, R. M. Fernandes, and V. Madhavan, *Nature* **631**, 60–66 (2024).
- [28] H. Deng, G. Liu, Z. Guguchia, T. Yang, J. Liu, Z. Wang, Y. Xie, S. Shao, H. Ma, W. Liège, F. Bourdarot, X.-Y. Yan, H. Qin, C. M. I. au2, R. Khasanov, H. Luetkens, X. Wu, G. Chang, J. Liu, M. H. Christensen, A. Kreisel, B. M. Andersen, W. Huang, Y. Zhao, P. Bourges, Y. Yao, P. Dai, and J.-X. Yin, *Evidence chain for time-reversal symmetry-breaking kagome superconductivity* (2024), arXiv:2408.02898 [cond-mat.supr-con].
- [29] Y. Xu, Z. Ni, Y. Liu, B. R. Ortiz, Q. Deng, S. D. Wilson, B. Yan, L. Balents, and L. Wu, *Nature Physics* **18**, 1470–1475 (2022).
- [30] Y.-P. Lin and R. M. Nandkishore, *Phys. Rev. B* **104**, 045122 (2021).
- [31] T. Park, M. Ye, and L. Balents, *Phys. Rev. B* **104**, 035142 (2021).
- [32] X. Feng, Y. Zhang, K. Jiang, and J. Hu, *Phys. Rev. B* **104**, 165136 (2021).

- [33] M. M. Denner, R. Thomale, and T. Neupert, *Phys. Rev. Lett.* **127**, 217601 (2021).
- [34] M. H. Christensen, T. Birol, B. M. Andersen, and R. M. Fernandes, *Phys. Rev. B* **106**, 144504 (2022).
- [35] H. Li, Y. B. Kim, and H.-Y. Kee, *Phys. Rev. Lett.* **132**, 146501 (2024).
- [36] K. Shimura, R. Tazai, Y. Yamakawa, S. Onari, and H. Kontani, *Journal of the Physical Society of Japan* **93**, 033704 (2024).
- [37] J.-W. Dong, Z. Wang, and S. Zhou, *Phys. Rev. B* **107**, 045127 (2023).
- [38] R. Tazai, Y. Yamakawa, and H. Kontani, *Nature Communications* **14**, 10.1038/s41467-023-42952-6 (2023).
- [39] W. Liège, Y. Xie, D. Bounoua, Y. Sidis, F. Bourdarot, Y. Li, Z. Wang, J.-X. Yin, P. Dai, and P. Bourges, *Search for orbital magnetism in the kagome superconductor CsV_3Sb_5 using neutron diffraction* (2024), [arXiv:2407.14391 \[cond-mat.str-el\]](https://arxiv.org/abs/2407.14391).
- [40] D. R. Saykin, C. Farhang, E. D. Kountz, D. Chen, B. R. Ortiz, C. Shekhar, C. Felser, S. D. Wilson, R. Thomale, J. Xia, and A. Kapitulnik, *Phys. Rev. Lett.* **131**, 016901 (2023).
- [41] J. Wang, C. Farhang, B. R. Ortiz, S. D. Wilson, and J. Xia, *Phys. Rev. Mater.* **8**, 014202 (2024).
- [42] C. Farhang, J. Wang, B. R. Ortiz, S. D. Wilson, and J. Xia, *Nature Communications* **14**, 10.1038/s41467-023-41080-5 (2023).
- [43] C. Guo, G. Wagner, C. Putzke, D. Chen, K. Wang, L. Zhang, M. Gutierrez-Amigo, I. Errea, M. G. Vergniory, C. Felser, M. H. Fischer, T. Neupert, and P. J. W. Moll, *Nature Physics* **20**, 579–584 (2024).
- [44] S. Blundell, R. De Renzi, T. Lancaster, and F. Pratt, *Muon Spectroscopy: An Introduction* (Oxford University Press, 2022).
- [45] L. Yu, C. Wang, Y. Zhang, M. Sander, S. Ni, Z. Lu, S. Ma, Z. Wang, Z. Zhao, H. Chen, K. Jiang, Y. Zhang, H. Yang, F. Zhou, X. Dong, S. L. Johnson, M. J. Graf, J. Hu, H.-J. Gao, and Z. Zhao, *arXiv preprints* (2021), 2107.10714.
- [46] R. Khasanov, D. Das, R. Gupta, C. Mielke, M. Elender, Q. Yin, Z. Tu, C. Gong, H. Lei, E. T. Ritz, R. M. Fernandes, T. Birol, Z. Guguchia, and H. Luetkens, *Phys. Rev. Res.* **4**, 023244 (2022).
- [47] Z. Guguchia, C. Mielke, D. Das, R. Gupta, J.-X. Yin, H. Liu, Q. Yin, M. H. Christensen, Z. Tu, C. Gong, N. Shumiya, M. S. Hossain, T. Gamsakhurdashvili, M. Elender, P. Dai, A. Amato, Y. Shi, H. C. Lei, R. M. Fernandes, M. Z. Hasan, H. Luetkens, and R. Khasanov, *Nature Communications* **14**, 153 (2023).
- [48] A. Abragam, *Compt. Rend. Acad. Sci. Ser. II* **299**, 95 (1984).
- [49] S. F. J. Cox, *Zeitschrift für Naturforschung A* **47**, 371–381 (1992).
- [50] J. N. Graham, C. M. III, D. Das, T. Morresi, V. Sazgari, A. Suter, T. Prokscha, H. Deng, R. Khasanov, S. D. Wilson, A. C. Salinas, M. M. Martins, Y. Zhong, K. Okazaki, Z. Wang, M. Z. Hasan, M. Fischer, T. Neupert, J. X. Yin, S. Sanna, H. Luetkens, Z. Salman, P. Bonfa, and Z. Guguchia, *arXiv preprints* (2024), 2402.11130.
- [51] S. Giblin, S. Cottrell, P. King, S. Tomlinson, S. Jago, L. Randall, M. Roberts, J. Norris, S. Howarth, Q. Mutamba, N. Rhodes, and F. Akeroyd, *Nuclear Instruments and Methods in Physics Research Section A: Accelerators, Spectrometers, Detectors and Associated Equipment* **751**, 70 (2014).
- [52] Z. Shan, P. K. Biswas, S. K. Ghosh, T. Tula, A. D. Hillier, D. Adroja, S. Cottrell, G.-H. Cao, Y. Liu, X. Xu, Y. Song, H. Yuan, and M. Smidman, *Phys. Rev. Res.* **4**, 033145 (2022).
- [53] W. Huang, V. Pacradouni, and J. Sonier, *Physics Procedia* **30**, 129 (2012), 12th International Conference on Muon Spin Rotation, Relaxation and Resonance ($\mu\text{SR}2011$).
- [54] P. Bonfà, J. Frassinetti, J. M. Wilkinson, G. Prando, M. M. Isah, C. Wang, T. Spina, B. Joseph, V. F. Mitrović, R. De Renzi, S. J. Blundell, and S. Sanna, *Phys. Rev. Lett.* **129**, 097205 (2022).
- [55] J. M. Wilkinson, F. Lang, P. J. Baker, S. P. Cottrell, and S. J. Blundell, *Journal of Physics: Conference Series* **2462**, 012007 (2023).
- [56] R. Kadono, W. Higemoto, A. Koda, K. Kakuta, K. Ohishi, H. Takagiwa, T. Yokoo, and J. Akimitsu, *Journal of the Physical Society of Japan* **69**, 3189 (2000).
- [57] A. Yaouanc and P. de Réotier, *Muon Spin Rotation, Relaxation, and Resonance: Applications to Condensed Matter*, International Series of Monographs on Physics (OUP Oxford, 2011).
- [58] Graham, J.N., Mielke III, C., Das, D., Morresi, T., Ardakani, V., Suter, A., Prokscha, T., Deng, H., Khasanov, R., Wilson, S. D., Salinas, A. C., Zhong, Y., Okazaki, K., Wang, Z., Hasan, M. Z., Fisher, M., Neupert, T., Yin, J.-X., Sanna, S., Luetkens, H., Salman, Z., Bonfà, P., and Guguchia, Z., *Depth-dependent time reversal symmetry breaking response in the charge-ordered kagome material RbV_3Sb_5* (2024).
- [59] Frassinetti, Jonathan, Bonfà, Pietro, Allodi, Giuseppe, Garcia, Erik, Cong, Rong, Ortiz, Brenden R., Wilson, Stephen D., De Renzi, Roberto, Mitrović, Vesna F., and Sanna, Samuele, *Microscopic nature of the charge-density wave in the kagome superconductor RbV_3Sb_5* (2024).
- [60] M. Celio, *Phys. Rev. Lett.* **56**, 2720 (1986).
- [61] P. Bonfà, J. Frassinetti, M. M. Isah, I. J. Onuorah, and S. Sanna, *Computer Physics Communications* **260**, 107719 (2021).
- [62] This is trivially the result of the larger dipolar contribution of the closest Sb nucleus with respect to the more distant V nuclei.
- [63] For the sake of consistency, we adopt the prediction of PW simulations for all parameters defining the interaction i.e. the distance between the muon and V atoms and the EFG at V sites. The latter values are averaged among the six nuclei and C_Q^{PW} and η^{PW} are 6.893 MHz and 0.164, respectively. The prediction for V_{zz} is very close to the one from APW simulations in the unperturbed lattice while the one for η deviates substantially: this is actually due to the limits of the computational basis rather than to perturbation effects. Indeed, unperturbed V nuclei far from the muon have $\eta \sim 0.2$ instead of $\eta \sim 0.4$. See supplemental materials for more details.
- [64] This value is computed by considering the half width half maximum of a Lorentzian distribution. A similar conclusion is also reached by considering the variation of the Δ parameter.
- [65] Q. Zhang, Y. Zhang, T. Wang, Z. Zhao, L. Zhou, B. Hou, H. Ji, H. Yang, T. Zhang, J.-T. Sun, H. Yang, H.-J. Gao, and Y. Wang, *Nano Letters* **24**, 6560 (2024).
- [66] F. Grandi, A. Consiglio, M. A. Sentef, R. Thomale, and D. M. Kennes, *Phys. Rev. B* **107**, 155131 (2023).
- [67] A. Dal Corso, *Computational Materials Science* **95**, 337 (2014).
- [68] J. P. Perdew, A. Ruzsinszky, G. I. Csonka, O. A. Vydrov, G. E. Scuseria, L. A. Constantin, X. Zhou, and K. Burke, *Phys. Rev. Lett.* **100**, 136406 (2008).
- [69] H. J. Monkhorst and J. D. Pack, *Phys. Rev. B* **13**, 5188 (1976).
- [70] D. Ceresoli, A. P. Seitsonen, U. Gerstmann, E. Kucukbenli, S. de Gironcoli, P. Giannozzi, N. Varini, M. Calandra, L. Paulatto, C. Cavazzoni, A. D. Corso, F. Spiga, and A. Ferreira, QE-GIPAW, <https://github.com/dceresoli/qe-gipaw> (2024), [Online; accessed 29-July-2024].

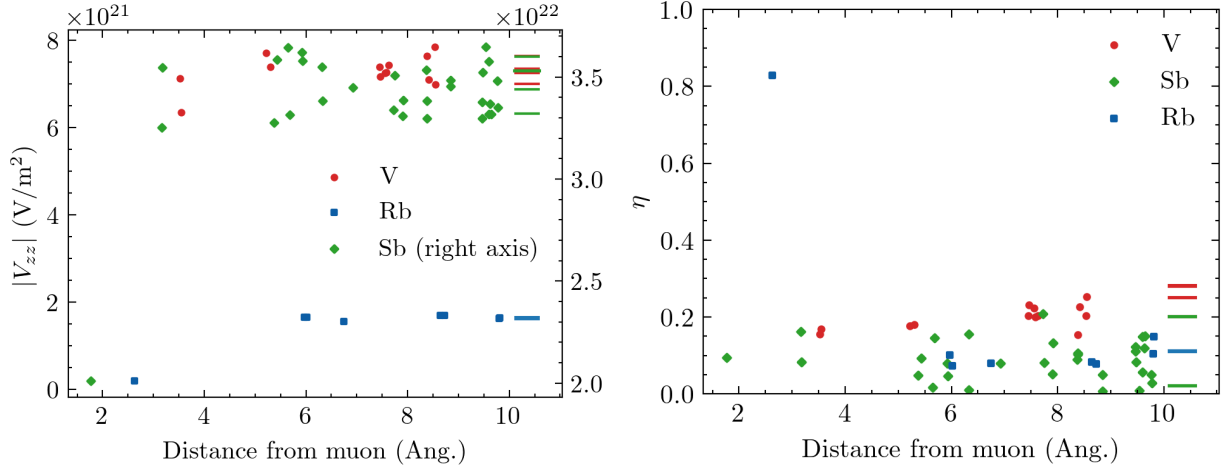


FIG. S1. The values of V_{zz} (left) and of the asymmetry parameter η (right) for each atom in the PW-based supercell simulation of Ref. [58] reported as a function of the distance from the muon site. The values for the unperturbed lattice in the tri-hexagonal phase are reported as colored thick bars on the right side of each plot.

SUPPLEMENTARY INFORMATION TO “UNVEILING THE NATURE OF ELECTRONIC TRANSITIONS IN RBV_3SB_5 WITH AVOIDED LEVEL CROSSING μSR ”

ANALYSIS OF EFG OBTAINED FROM PLANE-WAVE BASED SIMULATIONS

The embedding position of the positive muon and the perturbation that it induces on the Electric Field Gradient (EFG) of its neighboring atoms is obtained by analyzing the computational results published in Ref. [50]. The description of the local distortion of the lattice can be found in the supplemental information of the cited reference, the perturbation of the EFG at the nuclear sites is shown in Fig. S1. As shown in the figure, V_{zz} (the largest component of the EFG in the principal axis system) of the nearest neighbor (NN) Sb atom is strongly perturbed by the positive interstitial charge of the muon. The second NN, Rb, also shows a substantial reduction of V_{zz} while V atoms (red points) are almost unperturbed, with a small decrease of V_{zz} by less than 10 %. The asymmetry parameter η of the nearest Rb atom shows the largest deviation from the unperturbed value. At large distance, both V_{zz} and η for the various atoms reach the unperturbed values indicated by the dashed line in the figure (obtained with additional simulations using the same code and computational parameters reported in Ref. [50]).

The most accurate results for the EFG at V sites are obtained with a full-potential approach using augmented plane waves. Here we report the estimates provided in Ref.[7, 59] in the last two columns of Tab. SI which are used to produce Fig. 4a in the main text. Comparison can be made with the unperturbed values obtained for the same lattice structure with a PW based method (second and third columns of Tab. SI)

Atom	PW		APW	
	$ V_{zz} $ (10^{22} Vm^{-2})	η	$ V_{zz} $ (10^{22} Vm^{-2})	η
Sb	3.34	0.065	3.31	0.111
Sb	3.49	0.0	3.52	0.0
Sb	3.05	0.039	3.20	0.058
Sb	3.10	0.0	3.32	0.0
Rb	0.137	0	0.093	0.0
Rb	0.140	0.024	0.110	0.127
V	0.693	0.241	0.660	0.431
V	0.731	0.221	0.697	0.432

TABLE SI. Value of EFG parameters for the inequivalent nuclei in the Tri-Hexagonal structure as obtained from APW simulations.

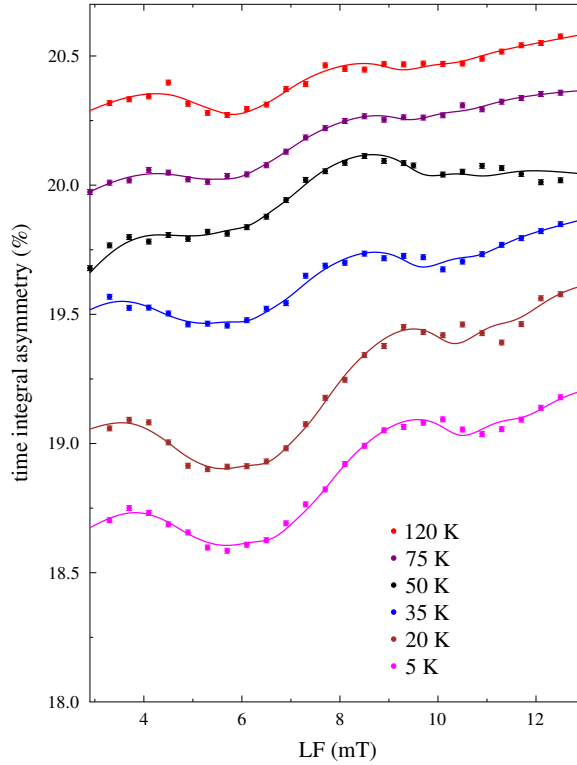


FIG. S2. Fit of time integrated asymmetry according to the model reported in the main text. Scans are displaced vertically for clarity.

T	NQCC factor (Err)	η (Err)	Amplitude (Err)	A0 (Err)	BG-lin (Err)	BG-quad (Err)	BG-cubic (Err)	χ^2
120	0.9034(62)	0.629(16)	0.852(50)	19.741(34)	0.0272(17)	-0.000306(23)	0.00000113(9)	4.439
75	0.9629(62)	0.451(14)	0.735(58)	19.291(30)	0.0184(17)	-0.000153(23)	0.00000045(9)	2.060
50	0.9871(37)	0.3889(56)	1.353(61)	19.277(29)	0.0421(16)	-0.000418(21)	0.00000126(9)	13.419
35	0.9826(38)	0.4020(63)	1.356(56)	19.432(30)	0.0339(16)	-0.000376(22)	0.00000138(9)	7.989
20	1.0525(24)	0.3919(36)	2.176(63)	19.532(31)	0.0202(17)	-0.000135(23)	0.00000033(9)	15.135
5	1.0685(26)	0.3928(39)	2.075(64)	19.283(31)	0.0290(17)	-0.000245(23)	0.00000072(9)	9.133

TABLE SII. Results of the fit shown in Fig. S2 and described in the main text.

PREDICTED RESONANCES AND FIT OF ALC RESONANCES

The ALC resonances are computed with two different approaches. In a first analysis, the interaction between the muon and a single nucleus is considered and the resulting asymmetry is integrated over the range 0 to 24 μ s. The results obtained for the NN Rb and Sb nuclei of the muon are shown in Fig. S3 and Fig. S4 respectively. From these it can be seen that the Rb QLCR spectrum is weak and at very low field and the Sb spectrum is also weak and at much higher field than our measurement range. Having ruled out contributions from these nuclei, the same approach is used in the main text to fit the experimental results considering only the contribution of V atoms. The resulting best fits are shown in Fig. S2 with corresponding values reported in Tab. SII and plotted in Fig.4b of the main text.

A second set of simulations is performed with the method proposed by Celio [60]. In this case we consider a larger Hilbert space which describes 6 V atoms and, in one case, also the nearest neighbor Sb atom of the muon. The powder average is performed using 500 random directions. The result is shown in Fig. 4a in the main text.

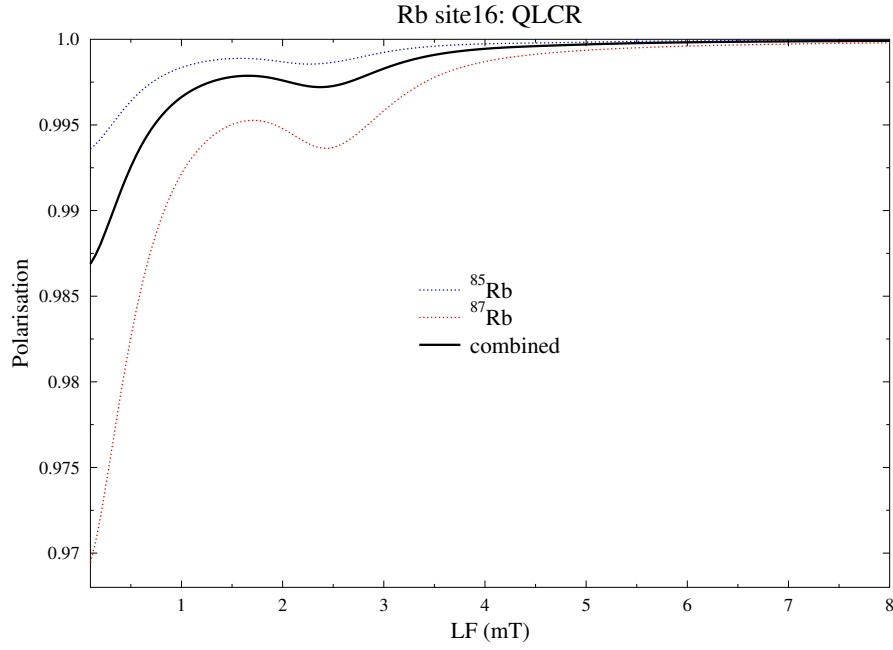


FIG. S3. Resonances predicted for Rb nuclei using the EFG tensors from PW-DFT simulations.

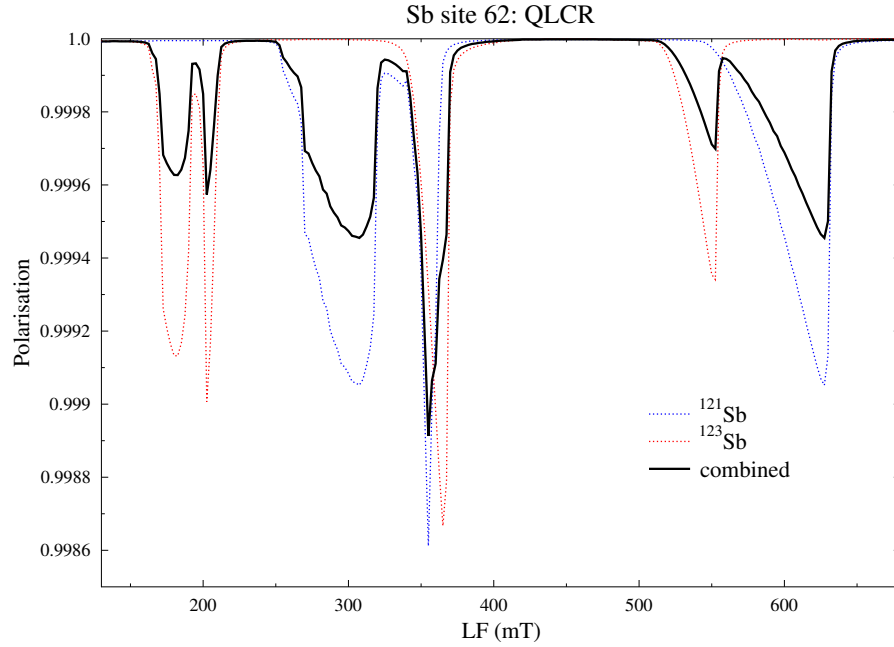


FIG. S4. Resonances predicted for Sb nuclei using the EFG tensors from PW-DFT simulations.

ADDITIONAL DFT SIMULATIONS

The values for the unperturbed EFG in the PW basis reported in Tab. SI are obtained using augmented plane wave pseudopotentials of the PSLibrary [67]. The PBEsol [68] functional has been used to approximate the exchange and correlation contribution and the reciprocal space has been sampled with a $8 \times 8 \times 8$ Monkhorst-Pack grid [69]. The plane wave cutoff is set

to 90 Ry while charge density is expanded up to 1020 Ry. The EFG tensors are obtained with the GIPAW code [70].